ISSN: 1410-8917
Jurnal Kimia Sains & Aplikasi
e-ISSN: 2597-9914

Jurnal Kimia Sains dan Aplikasi 29 (2) (2026): 82-100

Jurnal Kimia Sains dan Aplikasi
Journal of Scientific and Applied Chemistry

Journal homepage: http://ejournal.undip.ac.id/index.php/ksa

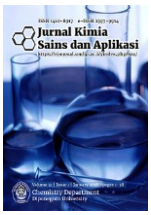

Rational Design of Cyanopyridine Derivatives as PIM-1 Kinase Inhibitors: *In Silico* Studies of QSAR, ADMET, and Interaction Analysis

Muhamad Jalil Baari [1,*], Salim [2], Firnayanti Mbuli [1]

[1] Department of Chemistry, Faculty of Science and Technology, Universitas Sembilanbelas November Kolaka, Kolaka, Indonesia
[2] Department of Mathematics, Faculty of Science and Technology, Universitas Sembilanbelas November Kolaka, Kolaka, Indonesia

* Corresponding author: jalilbaari@gmail.com

https://doi.org/10.14710/jksa.29.2.82-100

Article Info

Article history:

Received: 14th August 2025
Revised: 27th January 2026
Accepted: 05th February 2026
Online: 14th March 2026

Keywords:
Anti-breast cancer; Cyanopyridine derivatives; *In silico*; PIM-1 kinase; QSAR

Abstract

Breast cancer is one of the most prevalent diseases among women and ranks among the top five leading causes of cancer-related deaths worldwide. Current therapeutic approaches remain suboptimal in addressing the highly aggressive progression of cancer cells. A simple method to initiate the drug discovery process is Quantitative Structure-Activity Relationship (QSAR) analysis. Previous experimental studies have reported that cyanopyridine derivatives exhibit potent inhibitory effects on PIM-1 kinase, a key regulator in MCF-7 human breast cancer cells. In this study, we performed QSAR analysis on structurally modified cyanopyridine derivatives to design novel anti-breast cancer agents. The research methodology included: (1) molecular geometry optimization using the PM3 semi-empirical method, (2) calculation of QSAR descriptors (hydrophobic, electronic, and steric parameters), and (3) rational molecular design based on the derived QSAR model. Optimizations and calculations were performed using HyperChem software. Multiple Linear Regression (MLR) analysis and external validation generated the best QSAR equation for Model 1: $\log (1/IC_{50}) = 151.273 + 1884.726qC_1 - 4663.478qC_4 + 5431.564qC_5 + 1501.074qN_7 + 592.015qO_{10}$. This model exhibits better core statistical metrics, with an $R = 0.868$, $R^2 = 0.753$, SEE = 0.272, $R^2_{ext} = 0.9342$, and $Q^2_{ext} = 0.8717$. In addition, statistical parameters of the Y-scrambling test indicate the robustness of the best QSAR model (average $R_{scramble} = 0.3881$; average $R^2_{scramble} = 0.1558$). A promising drug candidate was identified based on antiproliferative activity predicted by the best QSAR model. A subsequent *in silico* evaluation comprehensively assessed their pharmacokinetic and toxicity profiles. The results revealed that synthesized and designed derivatives successfully satisfied most critical pharmaceutical criteria. The pharmacokinetic profile of this compound was comparable to the native ligand (VRV), as well as established reference drugs like tamoxifen and doxorubicin. 2-[4-(5-Cyano-6'-fluoro-1-methyl-6-oxo-1,6-dihydro-[2,3']bipyridinyl-4-yl)-2-methoxy-phenoxy]-*N*-phenyl-acetamide (8M) was considered the best potential drug candidate due to its high anti-breast cancer efficacy and relatively low toxicity. The molecular docking study demonstrates that the binding affinity of the designed cyanopyridine derivatives for the PIM-1 kinase receptor was in the range of -9.5 to -9.7 kcal·mol^{-1}, which is comparable to that of doxorubicin (10.0 kcal·mol^{-1}). Moreover, these values surpass the binding affinity of the native ligand (9.2 kcal·mol^{-1}) and tamoxifen (8.0 kcal·mol^{-1}). This finding was further corroborated by molecular dynamics simulations, which demonstrated the stability of the interactions. Therefore, these designed compounds have potential as novel anti-breast cancer drugs.

1. Introduction

Breast cancer is a heterogeneous disease at the molecular level, whose characteristics comprise human epidermal growth receptor (HER2) activation (encoded by ERBB2), hormone receptor signaling through estrogen receptor (ER) and progesterone receptor (PR), and potential BRCA gene mutations [1]. WHO reports indicate that breast cancer is the second most prevalent cancer worldwide and a major contributor to cancer-associated mortality [2, 3]. Moreover, there were 2.3 million cases of breast cancer in 2022, according to the Global Cancer Observatory. Although breast cancer is predominantly diagnosed in women, it can also develop in men. These ER, PR, and HER2-targeted therapies can still cure patients in the early stage without metastasis. On the other side, acquired resistance and incurable metastasis remain major challenges in breast cancer [4].

The Proviral Integration site for Moloney murine leukemia virus (PIM-1) kinase, frequently expressed as a key promoter of these challenges and linked to poor outcomes, directly drives these processes by conferring therapy resistance and promoting metastatic mechanisms such as Epithelial-Mesenchymal Transition (EMT) and invasion, thus representing a compelling therapeutic target beyond conventional receptors [5]. Various efforts have been applied to treat breast cancer patients, for instance, hormone therapy, chemotherapy, and surgical methods. These efforts focus on reducing HER2 protein in cancer treatment to disrupt oncogenic survival signaling pathways. Pharmacological inhibition of the PIM-1 kinase can also be a therapeutic target. However, those efforts have not significantly raised their life expectancy [6]. PIM-1 kinase plays a crucial role in tumor progression, metastasis, and chemotherapy resistance, making it a promising therapeutic target for cancer. Overexpression of PIM1 has been observed in various cancers, including breast, prostate, pancreatic, gastric, colorectal, leukemia, lung, and head and neck squamous cell carcinomas [7].

Chemotherapy is a widely used therapeutic modality in cancer treatment. This approach employs cytotoxic agents that selectively inhibit the activity of enzymes and proteins involved in cancer cell proliferation, such as PIM-1 kinase in breast cancer cases [8]. However, current chemotherapeutic drugs still demonstrate suboptimal therapeutic efficacy. Furthermore, cancer cell progression frequently induces resistance to specific anticancer agents. These limitations have prompted extensive research efforts to expand novel drug compounds with enhanced therapeutic effectiveness.

In silico drug discovery and design has emerged as a prominent contemporary methodology in modern drug development [9]. Computational approaches significantly reduce both time and cost in breast cancer drug discovery and enable reliable prediction of drug feasibility and potential adverse effects prior to clinical application. The effectiveness and toxicity of a drug compound are fundamentally dependent on its chemical structure. The addition of electronegative substituents, such as halogen atoms, hydroxyl, and alkoxy groups, affects changes in the activity of the natural compounds [10]. Consequently, several organic compounds, including pyridine, pyrimidine, parviflorons, quinazoline, and cyanopyridine derivatives, have been discovered and developed as potential therapeutic agents, particularly for breast cancer treatment [10, 11].

Meanwhile, structural analysis of novel drug compounds is typically performed using quantitative structure-activity relationship (QSAR) studies, pharmacokinetic assays, drug-likeness evaluation, molecular docking, and molecular dynamics simulation, or a combination of these approaches [12, 13]. These approaches can be conducted before *in vitro* and *in vivo* drug activity and feasibility testing, or as complementary methods for interpreting experimental results. This study employed an environmentally conscious, cost-effective approach by minimizing chemical use and animal experimentation. The methodology demonstrates high efficiency through computational strategies that incorporate mathematical modeling, specialized software, and web-based platforms to evaluate potential anticancer compounds.

An *in silico* method has been utilized to investigate thymoquinone derivatives as potential anti-breast cancer agents. Lipophilic and steric parameters are the prominent parameters that determine the activity of thymoquinone derivatives against the HER2 protein [14]. Besides that, inhibiting PIM-1 kinase is a protective measure against cancer proliferation. A study explained that the insertion of *N*,*N*-dimethyl phenyl group on the cyanopyridine could reduce prostate cancer cells after inhibiting PIM-1 kinase activity (IC_{50} < 1 µM) [15]. Another study has designed and synthesized novel amino alcohol derivatives to treat breast cancer cells (MCF-7) [16]. These compounds exhibit promising anticancer properties by inducing apoptosis in breast cancer cells through PIM-1 kinase inhibition.

In this study, we investigate cyanopyridine derivatives as potential breast cancer therapeutics using an in vitro method based on a previous study that synthesized and reported significant PIM-1 kinase inhibitory activity with IC_{50} values <10 µM [17]. Furthermore, we employ QSAR analysis to identify the optimal QSAR model and to elucidate the electronic, hydrophobic/lipophilic, and steric parameters that govern anticancer activity. After that, we conducted a rational design and a comprehensive *in silico* approach to enhance pharmacological efficacy by satisfying key drug development criteria, such as optimized pharmacokinetic properties (ADME), drug-likeness characteristics, toxicity, and specific binding interactions of novel cyanopyridine derivatives with PIM-1 kinase.

Despite the known oncogenic role of PIM-1 kinase in breast cancer progression and therapy resistance, the development of highly selective and potent molecule inhibitors remains a challenge. A significant research gap exists in the systematic, rational design of cyanopyridine-based scaffolds targeting this kinase. This study addresses that gap by employing an integrated computational strategy that combines QSAR, ADMET

profiling, and molecular interaction studies (molecular docking and molecular dynamics) to rationally design, prioritize, and optimize novel cyanopyridine derivatives before costly, time-consuming synthetic and biological evaluations.

2. Experimental

2.1. Materials and Equipment

The compounds, sourced from literature [17] were analyzed for their chemical structures (Figure 1) and biological activity. Table 1 displays the substituent variations and corresponding antiproliferative efficacy, expressed as half-maximal inhibitory concentration (IC_{50}) values.

A laptop equipped with an AMD Ryzen 7 6800H, 3.20 GHz processor with Radeon Graphics, 24 GB RAM, and 512 GB SSD was used as hardware. Meanwhile, the software consisted of ChemDraw Ultra 7.0, Avogadro version 1.2.0, HyperChem version 8.0, IBM(R) SPSS(R) version 22.0, SwissADME web server, ProTox-3.0 web server, AutoDockTools-1.5.7, BIOVIA Discovery Studio version 21.1, PyRx version 0.8, PyMOL version 3.02, CABS-flex 3.0, and iMOD server.

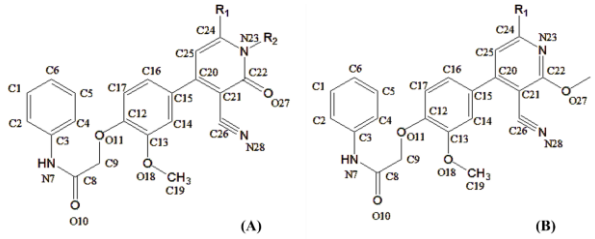

Figure 1. Chemical structure of cyanopyridine derivatives

Table 1. Description of the R_1, R_2, and cytotoxicity of cyanopyridine derivatives from the *in vitro* antiproliferative assays [17]

Sign	Compound	R_1	R_2	Cytotoxicity, IC_{50} (μM)	log IC_{50}	Calc. log IC_{50}
A	1	C_6H_5–	H	8.06	5.09366	5.29435
A	2	3-MeO–C_6H_4–	H	56.813	4.24558	4.29978
A	3	4-MeO–C_6H_4–	H	7.72	5.11238	4.83461
A	4	4-Cl–C_6H_4–	H	41.126	4.38584	4.54595
A	5	4-Br–C_6H_4–	H	21.91	4.65936	4.62598
A	6	2-furyl	H	3.98	5.40012	5.37938
A	7	2-thiophenyl	H	1.93	5.71444	5.64316
A	8	3-pyridyl	H	1.89	5.72354	5.06063
A	9	4-pyridyl	H	23.95	4.62069	4.85964
A	10	2-Naphthyl	H	20.09	4.69702	4.51837
A	11	C_6H_5–	CH_3	9.1	5.04096	4.96238
A	12	3-MeO–C_6H_4–	CH_3	8.8	5.05552	4.87285
A	13	4-MeO–C_6H_4–	CH_3	26.07	4.58386	5.12689
A	14	4-Cl–C_6H_4–	CH_3	2.053	5.68761	5.27287
A	15	4-Br–C_6H_4–	CH_3	18.28	4.73802	4.86219
A	16	2-Naphthyl	CH_3	41.42	4.38279	4.54849
A	17	2-furyl	CH_3	13.2	4.87943	5.06743
B	18	C_6H_5–	–	14.28	4.84527	4.64070
B	19	3-MeO–C_6H_4–	–	36.19	4.44141	4.62468
B	20	4-MeO–C_6H_4–	–	3.75	5.42597	5.63769
B	21	4-Cl–C_6H_4–	–	17.97	4.74545	4.74158
B	22	4-Br–C_6H_4–	–	42.64	4.37018	4.47229
B	23	2-Naphthyl	–	1.7	5.76955	5.84727
B	24	2-furyl	–	21.25	4.67264	4.62592
B	25	$C_5H_4NCH_3I$	–	2.14	5.66959	5.60572

2.2. Geometry Optimization and Descriptor Calculation

Geometry optimization was performed on the molecular structures of 25 cyanopyridine derivatives, followed by calculation of QSAR descriptors using HyperChem 8.0. These descriptors consisted of hydrophobic/lipophilic, electronic, and steric parameters. Electronic descriptors included atomic charges in cyanopyridine derivatives, dipole moment (DM), LUMO and HOMO energies, and polarizability (α). The partition coefficient (log P) characterizes a molecule's relative hydrophobicity or lipophilicity properties [18]. The steric properties were characterized by molecular weight (MW) and molar refractivity (MR). The calculations applied the semi-empirical Parametric Method 3 (PM3) for quantum chemical analysis [19]. This method was employed owing to its greater relevance in characterizing the system's physicochemical aspects [20]. The convergence criterion was established at 0.001 kcal/Å·mol gradient tolerance using the Polak–Ribiere optimization algorithm [21]. This analysis generated a mathematical model characterizing the quantitative relationship between selected molecular descriptors and antiproliferative activity.

The best QSAR equation was subsequently employed to predict the IC_{50} values of newly designed derivative compounds. Before establishing the QSAR equation, bivariate correlation analysis was first conducted to identify the molecular descriptors exhibiting the most significant relationship with anticancer activity, expressed as $\log(1/IC_{50})$. This procedure was implemented to reduce overrepresented molecular descriptors, particularly by eliminating redundant atomic net charge parameters in the cyanopyridine derivatives.

The QSAR modeling was developed using multiple linear regression (MLR) analysis, with molecular descriptors as independent variables and antiproliferative activity (expressed as $\log(1/IC_{50})$) as the dependent variable. The backward elimination method was employed, which initially incorporates all potential descriptors and subsequently removes those showing insignificant correlation with the antiproliferative activity. This stepwise refinement process yielded an optimized regression equation with improved predictive capability.

2.3. Validation of the QSAR Model and Design of New Cyanopyridine Derivatives

The best QSAR equation was selected through statistical analysis performed in IBM® SPSS® version 22.0. Model validity was evaluated using statistical parameters, including the standard error of the estimate (SEE), correlation coefficient (R), coefficient of determination (R^2), adjusted R^2, predicted residual sum of squares (PRESS), and F-test ratio (F_{calc}/F_{table}) [22]. Furthermore, external validation was carried out by splitting the dataset into training and test sets using random partitioning. This validation assessed the coefficient of determination for external validation (R^2_{ext}), external predictive validity (Q^2_{ext}), PRESS, mean absolute error (MAE), mean squared error (MSE), and observed-to-predicted ratio (O/P ratio).

The final $\log(1/IC_{50})$ predictions were derived from the best and validated model. To further evaluate the model's robustness, a Y-randomization (Y-scrambling) test was performed, measuring the following parameters from the randomized models: the mean correlation coefficient ($R_{scramble}$) and mean squared correlation coefficient ($R^2_{scramble}$). Then, new cyanopyridine derivatives were designed based on descriptors that contribute significantly through the insertion of several substituents on the initial cyanopyridine derivative, with the strongest experimental activity and molecular weight < 500 Da.

2.4. Prediction of Drug-Likeness, Pharmacokinetics, and Toxicity of Drug Candidates

The evaluation of drug-likeness and pharmacokinetic properties was conducted using the SwissADME web tool (https://www.swissadme.ch/index.php), which incorporates the BOILED-Egg model to assess gastrointestinal (GI) absorption and blood–brain barrier (BBB) penetration [23, 24]. This platform provided a comprehensive analysis of ADME characteristics. Drug-likeness was evaluated according to multiple established criteria, including Lipinski's Rule of Five, Ghose, Veber, Egan, and Muegge rules. Additionally, toxicity endpoints, organ toxicity, toxicity class, and median lethal dose (LD_{50}) predictions were generated using the ProTox-III web server (https://tox.charite.de/protox3/) to screen potential drug candidates [25].

2.5. Molecular Docking Study

The native ligand, positive control, and newly designed cyanopyridine derivatives were docked into the PIM-1 kinase receptor (PDB ID: 2OBJ). Before docking, the receptor structure was prepared in AutoDock Tools and Discovery Studio by adding polar hydrogen and removing water molecules and native ligands [26, 27]. The docking protocol was validated through redocking experiments performed in PyRx using VRV as the native ligand [28, 29]. The grid box dimensions were set to 20 × 20 × 21 $Å^3$ and centered on the active binding site, with the exhaustiveness parameter set to 125. Docking accuracy was assessed using the root mean square deviation (RMSD) in PyMOL, where values < 2.0 Å indicated acceptable ligand pose reproduction [30], with lower RMSD values corresponding to better prediction of the native conformation [31]. The same docking parameters were subsequently applied to the designed compounds. Binding affinities ($kcal·mol^{-1}$) were calculated using PyRx, and protein–ligand interactions were visualized in Discovery Studio.

2.6. Molecular Dynamics Simulation Analysis

Molecular dynamics (MD) simulations were performed to analyze the structural dynamics of the PIM-1 kinase receptor in its unbound form and in complex with the best-designed ligands. Structural flexibility of the receptor was evaluated using the CABS-flex 3.0 web server (https://lcbio.pl/cabsflex3/?form=flexibility). The CABS-flex web server utilizes a coarse-grained (CG) modeling approach that requires only a single protein

structure in PDB format as input. The simulation protocol was configured with specific parameters, including the relative weighting of Cα and side-chain interactions, protein flexibility constraints, the number of simulation cycles, structural restraint settings, trajectory sampling parameters, the temperature regulation range, and the random number generator (RNG) seed initialization.

All remaining parameters were maintained at their default values throughout the simulation process. The structural dynamics (flexibility and stability) of the PIM-1 kinase receptor and its complexes with the selected derivatives were further analyzed using the iMODS web server (http://imods.chaconlab.org) [32, 33]. This platform performs normal mode analysis (NMA) on docked complexes to evaluate deformability, eigenvalues, B-factors, and elastic network properties. The analysis generates coarse-grained (CG) models using protein structures provided in .pdb format as input.

3. Results and Discussion

This study employed quantum mechanical calculations using the semi-empirical PM3 method to optimize the molecular geometry of cyanopyridine derivatives. The analysis included both previously synthesized compounds and 13 newly designed derivatives considered from QSAR modeling results. The semi-empirical PM3 method can compute formation enthalpies and optimize molecular geometries for organic molecules, including cyanopyridine derivatives [34]. The geometrically optimized structures were subjected to further analysis to compute molecular descriptors, for instance, frontier molecular orbital energies (HOMO/LUMO), net atomic charges, dipole moment, and QSAR-related parameters.

3.1. QSAR Equation Analysis

Eight structural descriptors with the most significant correlation to antiproliferative activity were used as independent variables, whereas antiproliferative activity (expressed as $\log(1/IC_{50})$) was used as the dependent variable in the QSAR model. These descriptors represent electronic and hydrophobic parameters. The computed values for all molecular descriptors are systematically presented in Table 2. Subsequent multivariate statistical analysis utilizing MLR was performed to develop QSAR models elucidating the quantitative contribution of individual descriptors to antiproliferative activity. As a result, four QSAR models were established, each demonstrating a fairly significant relationship between $\log(1/IC_{50})$ and selected molecular descriptors, as summarized in Tables 3 and 4.

Table 2. Molecular descriptors used for QSAR analysis of cyanopyridine derivatives as anti-breast cancer agents calculated using the semi-empirical PM3 method

Compound	Atomic net charges (Coulomb)						E_{LUMO} (eV)	log P
	qC_1	qC_4	qC_5	qC_6	qN_7	qO_{10}		
1	-0.0889	-0.1239	-0.0761	-0.1110	0.0419	-0.1877	-1.404	-1.92
2	-0.0885	-0.1234	-0.0760	-0.1110	0.0424	-0.1784	-1.43	-2.91
3	-0.0884	-0.1237	-0.0761	-0.1115	0.0421	-0.1788	-1.369	-2.91
4	-0.0886	-0.1235	-0.0760	-0.1112	0.0423	-0.1786	-1.508	-2.14
5	-0.0887	-0.1235	-0.0760	-0.1112	0.0424	-0.1786	-1.533	-1.87
6	-0.0882	-0.1233	-0.0758	-0.1087	0.043	-0.1784	-1.589	-3.65
7	-0.0883	-0.1233	-0.0757	-0.1090	0.0429	-0.1785	-1.642	-3.31
8	-0.0887	-0.1236	-0.0760	-0.1115	0.0423	-0.1788	-1.589	-3.27
9	-0.0888	-0.1233	-0.0758	-0.1111	0.0425	-0.1785	-1.623	-3.39
10	-0.0884	-0.1236	-0.0761	-0.1113	0.0422	-0.1786	-1.457	-1.84
11	-0.0885	-0.1238	-0.0761	-0.1116	0.042	-0.1788	-1.240	-1.67
12	-0.0888	-0.1238	-0.0762	-0.1103	0.0426	-0.1913	-1.206	-2.67
13	-0.0882	-0.1234	-0.0758	-0.1093	0.0426	-0.1784	-1.145	-2.67
14	-0.0884	-0.1233	-0.0757	-0.1096	0.0427	-0.1783	-1.227	-1.9
15	-0.0886	-0.1236	-0.0760	-0.1115	0.0422	-0.1788	-1.325	-1.62
16	-0.0884	-0.1238	-0.0762	-0.1116	0.042	-0.1789	-1.235	-1.6
17	-0.0889	-0.124	-0.0762	-0.1112	0.0418	-0.1878	-1.39	-3.41
18	-0.0885	-0.1239	-0.0764	-0.1102	0.0426	-0.1918	-1.118	-0.85
19	-0.0885	-0.1238	-0.0764	-0.1100	0.0429	-0.1916	-1.13	-1.84
20	-0.0885	-0.1237	-0.0761	-0.1089	0.0428	-0.1918	-1.099	-1.84
21	-0.0887	-0.1239	-0.0764	-0.1102	0.0428	-0.1918	-1.227	-1.07
22	-0.0885	-0.1238	-0.0763	-0.1113	0.0422	-0.1793	-1.284	-0.8
23	-0.0883	-0.124	-0.0762	-0.1114	0.042	-0.1793	-1.2266	-0.78
24	-0.0882	-0.124	-0.0764	-0.1113	0.0421	-0.179	-1.297	-2.58
25	-0.0883	-0.1246	-0.0765	-0.1108	0.0411	-0.18	-1.842	-1.62

Table 3. Coefficient of selected independent variables for four QSAR models obtained from MLR analysis

QSAR Model	Coefficient of independent variables								
	Constant	qC_1	qC_4	qC_5	qC_6	qN_7	qO_{10}	E_{LUMO}	log P
1	151.273	1884.726	-4663.478	5431.564	-	1501.074	592.015	-	-
2	-343.247	-	-5258.767	5359.370	-258.858	1797.849	-	-0.573	-
3	-204.227	-	-3887.982	4152.534	-	1029.952	-	-0.573	0.0629
4	-207.801	-	-3899.629	4082.244	-	1014.626	7.265	-0.4497	-

Table 4. Statistical parameters of four selected QSAR models correlating molecular descriptors with antiproliferative activity of cyanopyridine derivatives

QSAR Model	Descriptors	R	R^2	R^2_{adj}	SEE	F_{calc}/F_{tab}	PRESS
1	qC_1, qC_4, qC_5, qN_7, qO_{10}	0.868	0.753	0.688	0.272	4.236	1.4087
2	qC_4, qC_5, qC_6, qN_7, E_{LUMO}	0.856	0.732	0.662	0.284	3.792	1.5296
3	qC_4, qC_5, qN_7, log P, E_{LUMO}	0.832	0.692	0.611	0.304	3.115	1.7597
4	qC_4, qC_5, qN_7, qO_{10}, E_{LUMO}	0.828	0.685	0.602	0.307	3.016	1.7989

Table 5. External validation of QSAR models using training and test set data

QSAR Model	R^2_{ext}	Q^2_{ext}	O/P ratio	PRESS	MAE	MSE
1	0.9342	0.8717	1.0034	0.1186	0.1348	0.0237
2	0.8632	0.7334	1.0234	0.2465	0.1914	0.0493
3	0.7885	0.5878	1.0239	0.3811	0.1974	0.0762
4	0.7799	0.5713	1.0234	0.3964	0.2047	0.0793

The developed QSAR models demonstrated passable internal validity, as evidenced by statistical parameters including R, R^2, and adjusted R^2, SEE, F-test ratio (F_{calc}/F_{table}), and PRESS. These metrics collectively indicate a strong relationship and influence between molecular descriptors and the antiproliferative activity of cyanopyridine derivatives. Furthermore, external validation confirmed the model's reliability and predictive power, verifying its applicability for prospective compound screening. Model validity was established based on the following criteria: $R^2_{ext} > 0.6$ for model consistency, $Q^2_{ext} > 0.5$ for external predictability, minimal PRESS, MSE, MAE, and observed-to-predicted (O/P) ratio approaching unity. The external validation parameters for all QSAR models are presented in Table 5.

Four models obtained from multiple linear regression show that all models have a good relationship between molecular properties and antiproliferative activity. The best QSAR equation is found in model 1: $\log(1/IC_{50}) = 151.273 + 1884.726qC_1 - 4663.478qC_4 + 5431.564qC_5 + 1501.074qN_7 + 592.015qO_{10}$. The selection of Model 1 was based on the values of internal statistical parameters and external validation. All developed models maintained satisfactory predictive performance, as evidenced by coefficient of determination (R^2) values exceeding 0.6. The high R and R^2 approaching 1.0 demonstrate significant contributions of electronic and hydrophobic descriptors to the observed antiproliferative activity.

Model 1 shows reliable predictive capability (adjusted $R^2 = 0.688$). This metric compensates for the inclusion of multiple descriptors, ensuring that redundant or irrelevant independent variables do not artificially enhance model performance. Model 1 also exhibited lower SEE and PRESS values [35], indicating a small deviation between experimental and predicted antiproliferative activities. In addition, the values of F_{calc}/F_{tab} for all models are greater than 1, indicating a significant relationship between the descriptors and antiproliferative activity at a 95% confidence level. All molecular descriptors incorporated in the selected QSAR model demonstrate statistically good contributions to the antiproliferative activity (IC_{50}) of cyanopyridine derivatives.

Among all developed models, Model 1 demonstrated better predictive performance. It has the highest R^2, R^2_{ext}, adjusted R^2, and Q^2_{ext} values compared to other models. Besides that, it has the lowest PRESS, MAE, MSE, and O/P ratio. These validation metrics confirm the model's strong concordance with experimental $\log(1/IC_{50})$ values. The statistically significant descriptors identified in this optimal QSAR equation provide critical structural insights for the rational design of enhanced-potency cyanopyridine derivatives. A Y-scrambling test was performed to verify the robustness of the developed QSAR model and to ensure that its predictive power was not a product of chance correlation [36]. In this test, the antiproliferative activity data were randomly permuted against the fixed molecular descriptors to generate multiple randomized models. As per established validation guidelines [37], a reliable model must demonstrate significantly greater predictive ability than these scrambled models, which typically show poor performance in the absence of a true structure-activity relationship.

Table 6. Proposed new anti-breast cancer compounds and predicted IC_{50} values calculated using the best QSAR model

No.	Compound	R_1	R_2	Cytotoxicity, IC_{50} (μM)	$\log(1/IC_{50})$
1	8A	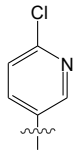	CH_3	24.5730	4.60954
2	8B	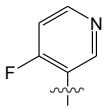	H	21.0904	4.67592
3	8C	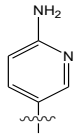	H	32.0996	4.49350
4	8D	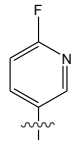	H	42.5857	4.37074
5	8E	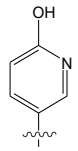	H	15.1430	4.81979
6	8F	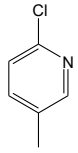	H	55.8635	4.25287
7	8G	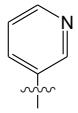	CH_3	27.9928	4.55295
8	8H	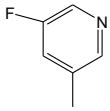	H	32.0010	4.49484
9	8I	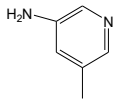	H	36.9385	4.43252
10	8J	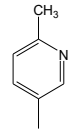	H	13.4171	4.87234
11	8K	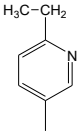	H	56.3688	4.24896
12	8L	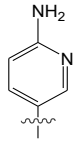	CH_3	9.293	5.03186
13	8M	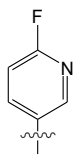	CH_3	4.7958	5.31914

The 30 randomized models demonstrated substantially reduced performance, with average R and R^2 values of 0.3881 and 0.1558, respectively. These low metrics indicate the absence of meaningful predictive capacity and structure–activity correlation in the scrambled models. Consistent with the previous studies, these findings support the lack of chance correlation, as their established thresholds ($R^2_{scramble} < 0.3$) were clearly unmet in the present anti-proliferative dataset [38, 39].

Table 1 presents the antiproliferative activity of cyanopyridine derivatives against breast cancer cells, as determined by an in vitro assay, along with the best QSAR model. The results indicate that bioactivity variations depend on the substituent types at carbons 24 and nitrogen 23. Notably, the insertion of 2-thiophenyl, 3-pyridyl, 2-Naphthyl, and $C_5H_4NCH_3I$ groups significantly reduces the log IC_{50} to below 2 µM. Consequently, the molecular design was focused on Compound 8, which exhibits the lowest IC_{50} value and molar mass < 500 Da, to develop potential breast cancer agents. The design strategy was guided by the predicted activity of each compound, as derived from descriptors in Model 1, which was the best QSAR model in this study. Additionally, considerations included synthetic feasibility, reactant availability, molecular mass, and structural simplicity. The substituent types and calculated bioactivities of the designed molecules are summarized in Table 6.

Regarding their antiproliferative activity (IC_{50}), the proposed Compound 8M exhibits superior activity compared to the other derivatives. These designed compounds demonstrate lower calculated IC_{50} values than Compound 8 and the remaining analogs. The introduction of an additional substituent, such as fluorine at the C_4 position of the 3-pyridyl group and a methyl group in atom N_{23} (R_2), enhances the bioactivity of the cyanopyridine framework. In contrast, attaching similar substituents to a similar cyanopyridine derivative with a hydrogen atom in R_2 tends to reduce antiproliferative efficacy due to a deficiency of charge transfer.

The value of E_{LUMO} plays a significant role in charge transfer and influences antiproliferative activity [40]. Electron-withdrawing substituents such as fluorine (F) and chlorine (Cl) decrease E_{LUMO} (i.e., make it more negative), thereby enhancing electron affinity and charge-transfer interactions. These improvements facilitate stronger non-covalent interactions with the amino acid residues of PIM-1 kinase via hydrogen bonding, π-π stacking, π-σ, π-alkyl, and van der Waals interactions. However, the QSAR models obtained showed that E_{LUMO} has no significant effect on activity. The insertion of fluorine at C_4 of the 3-pyridyl group produces the highest log ($1/IC_{50}$) among other designed compounds. It can also enhance polarizability and refractivity.

The presence of a bulky substituent, such as CH_3 for cyanopyridine derivatives with a 3-pyridyl group in the R_2 site, generally supports the increase of log($1/IC_{50}$) rather than a hydrogen atom. The observed effect may result from charge transfer, which reduces the negative charge on qC_5. Meanwhile, the presence of fluorine as a substituent in the C_4 position of the 3-pyridyl group shows better cytotoxicity than the C_l substituent. This position supports the more significant increase of log ($1/IC_{50}$) due to higher net charge distribution on the C_4, C_5, and N_7 atoms.

The partition coefficient (log P) serves as a critical parameter in drug design, governing intestinal membrane permeability following oral administration [41]. Optimal lipophilicity is essential, as excessively high log P values promote compound accumulation within lipid bilayers, leading to undesirable tissue retention [42]. Conversely, insufficient lipophilicity (low log P) compromises membrane absorption, impairing cellular transport and permeation efficiency [43, 44, 45]. Molecular mass is another key physicochemical determinant of membrane permeability. Compounds with molecular mass < 500 Da generally exhibit improved transmembrane diffusion due to reduced steric hindrance. Further discussion of these descriptors is provided in the section on drug-likeness and pharmacokinetic properties.

3.2. Prediction of Drug-Likeness and Pharmacokinetics Profiling

The drug-likeness assessment was performed using the SwissADME web server to evaluate potential drug candidates based on their pharmacokinetic properties and established drug-likeness filters from major pharmaceutical frameworks [23]. The evaluation applied Lipinski, Ghose, Veber, Egan, and Muegge rules. Lipinski's rule of five (RO5) evaluates small molecules based on key physicochemical parameters: molecular weight (MW) < 500 Da, no more than 10 hydrogen bond acceptors (N or O atoms), no more than 5 hydrogen bond donors (NH or OH groups), and an octanol–water partition coefficient (MLOGP) ≤ 4.15 [42]. According to RO5, a compound is unlikely to exhibit good oral bioavailability if it violates two or more of these criteria [46].

Ghose's rule evaluates drug-likeness based on defined physicochemical boundaries [47]. Drug-like compounds should satisfy the following criteria: MW between 160 and 480 Da, molar refractivity between 40 and 130, WLOGP between -0.4 and 5.6, and a total atom count between 20 and 70 atoms [48]. Veber's rule emphasizes oral bioavailability by restricting the number of rotatable bonds to ≤ 10, as excessive molecular flexibility may reduce membrane permeability. In addition, the total number of hydrogen bond donors and acceptors combined should be ≤ 12, and the topological polar surface area (TPSA) should be ≤ 140 Å^2, since lower TPSA generally enhances membrane permeation.

Egan's rule focuses on intestinal absorption potential and passive diffusion across biological membranes. It establishes two principal criteria: TPSA ≤ 131.6 Å^2 and WLOGP ≤ 5.88 to ensure adequate absorption [49]. Muegge's rule defines broader drug-likeness criteria: MW 200–600 Da, TPSA ≤ 150 Å^2, XlogP -2 to 5, at least one heteroatom, ≤ 7 rings, ≤ 10 hydrogen bond acceptors, ≤ 5 hydrogen bond donors, < 15 rotatable bonds, and ≥ 4 carbon atoms [47].

Table 7. Drug-likeness evaluation of cyanopyridine derivatives, native ligand (VRV), and reference drugs

Drug Candidate	Drug-likeness (Violation)					Bioavailability Score	Synthetic accessibility
	Lipinski	Ghose	Veber	Egan	Muegge		
8	Yes (0)	Yes (0)	Yes (0)	Yes (0)	Yes (0)	0.55	3.46
8A	Yes (1, MW>500)	No (2, MW>480, MR>130)	Yes (0)	Yes (0)	Yes (0)	0.55	3.66
8B	Yes (0)	Yes (0)	Yes (0)	Yes (0)	Yes (0)	0.55	3.59
8C	Yes (0)	No (1, MR>130)	No (1, TPSA >140)	No (1, TPSA >131.6)	Yes (0)	0.55	3.57
8D	Yes (0)	Yes (0)	Yes (0)	Yes (0)	Yes (0)	0.55	3.56
8E	Yes (0)	Yes (0)	Yes (0)	No (1, TPSA >131.6)	Yes (0)	0.55	3.55
8F	Yes (0)	No (2, MW>480, MR>130)	Yes (0)	Yes (0)	Yes (0)	0.55	3.54
8G	Yes (0)	No (1, MR>130)	Yes (0)	Yes (0)	Yes (0)	0.55	3.58
8H	Yes (0)	Yes (0)	Yes (0)	Yes (0)	Yes (0)	0.55	3.51
8I	Yes (0)	No (1, MR>130)	No (1, TPSA >140)	No (1, TPSA >131.6)	Yes (0)	0.55	3.55
8J	Yes (0)	No (1, MR>130)	Yes (0)	Yes (0)	Yes (0)	0.55	3.58
8K	Yes (0)	No (2, MW>480, MR>130)	Yes (0)	Yes (0)	Yes (0)	0.55	3.66
8L	Yes (0)	No (2, MW>480, MR>130)	Yes (0)	No (1, TPSA >131.6)	Yes (0)	0.55	3.69
8M	Yes (0)	No (2, MW>480, MR>130)	Yes (0)	Yes (0)	Yes (0)	0.55	3.68
VRV	Yes (0)	Yes (0)	Yes (0)	Yes (0)	Yes (0)	0.55	2.78
Doxorubicin	No (3, MW>500, N or O>10, NH or OH>5)	No (2, MW>480, MR>130)	No (1, TPSA >140)	No (1, TPSA >131.6)	No (3, TPSA >150, H-acc >10, H-don >5)	0.17	5.88
Tamoxifen	Yes (1, MLOGP >4.15)	No (1, WLOGP >5.6)	Yes (0)	No (1, WLOGP >5.88)	No (1, XLOGP3 >5)	0.55	3.01

Table 7 presents the drug-likeness evaluation of the cyanopyridine derivatives based on five established medicinal chemistry rules. Although most parameters were fulfilled across the designed compounds, deviations in MW, MR, and TPSA were observed in several derivatives.

Compounds 8, 8B, 8D, 8H, and VRV demonstrated full compliance with all drug-likeness criteria. Meanwhile, derivatives 8A, 8E, 8F, 8G, 8J, 8K, and 8M exhibited only a single violation of the five established rules. Such minor deviations do not necessarily compromise oral drug potential and indicate that these compounds remain promising candidates for further investigation.

This potential is further supported by favorable bioavailability scores of 0.55. Bioavailability, defined as the fraction and rate at which an administered drug reaches systemic circulation [50], influences both the onset and magnitude of therapeutic effects. The bioavailability score specifically predicts whether a compound achieves at least 10% oral bioavailability in mice or demonstrates measurable permeability in Caco-2 cells assays [23]. These human colon adenocarcinoma-derived cells serve as an *in vitro* model for studying intestinal drug absorption through dual transport

pathways. Compounds with bioavailability scores ≥ 0.55 are considered to have optimal absorption characteristics [51]. Another evaluated parameter was synthetic accessibility (SA), which computationally estimates the feasibility of chemical synthesis by considering molecular complexity, fragment contributions, precursor availability, and synthetic route length [52, 53]. SA values are expressed on a scale of 1–10, where lower scores indicate greater synthetic tractability, in accordance with conventional practice [54].

The pharmacokinetic profiling of cyanopyridine derivatives was conducted to evaluate their ADME characteristics. This comprehensive analysis aims to elaborate on the compound's behavior from oral administration through systemic circulation to ultimate excretion. These pharmacokinetic parameters are presented in Table 8. All designed cyanopyridine derivatives exhibit limited BBB permeability. The BBB represents a highly selective semipermeable interface that rigorously regulates molecular exchange between the circulatory and the central nervous system (CNS). This specialized barrier controls the passage of nutrients, therapeutic agents, and metabolic waste products while maintaining cerebral homeostasis [55].

All cyanopyridine derivatives were predicted to be substrates for CYP2C19, CYP2C9, and CYP3A4 isoenzymes, suggesting that these molecules may be metabolized via multiple cytochrome P450 pathways. CYP3A4 is known to contribute to the metabolism of Tamoxifen to its active metabolite, endoxifen, in the liver and small intestine. Tamoxifen is initially metabolized to 4-hydroxy-tamoxifen primarily by CYP2C19 and CYP2C9 [56], followed by further conversion to endoxifen mediated by CYP3A4. Meanwhile, most designed compounds were predicted not to be substrates of CYP1A2. This characteristic may reduce the likelihood of CYP1A2-mediated drug–drug interactions. However, further experimental validation would be required to confirm this prediction. A compound is generally considered a favorable oral drug candidate when it meets the following pharmacokinetic criteria: high gastrointestinal (GI) absorption, no BBB permeability (for non-CNS targets), non-substrate of P-glycoprotein (P-gp), and log K_p < -2.5 (cm/s), where log K_p represents the logarithm of the skin permeability coefficient.

The pharmacokinetic profiles included Boiled-Egg predictive modeling to simultaneously assess two critical parameters: (1) BBB penetrability and (2) gastrointestinal (GI) passive absorption potential [24]. In the Boiled-Egg plot (Figure 2), compounds 8A and 8F are highlighted in red, indicating a low capability for passive BBB penetration that is not affected by P-glycoprotein (P-gp). This classification is supported by their "No" P-gp substrate status in the pharmacokinetic analysis (Table 8). Thus, those compounds are not *P*-glycoprotein substrates. On the other hand, the remaining derivatives are predicted as *P-gp* substrates, allowing their active flux from the brain and the gastrointestinal tract into the lumen [55]. The ability of a drug candidate to cross the BBB presents a dual consideration in breast cancer therapy. While BBB penetration is highly desirable for treating or preventing brain metastases, which are common and devastating complications in advanced disease. But it may pose an unnecessary risk of CNS toxicity when treating early-stage, non-metastatic breast cancer, where the brain is not a target organ.

Table 8. Predicted pharmacokinetic parameters of designed cyanopyridine derivatives and reference compounds

Compound	GI Absorption	BBB Permeant	P-gp Substrate	Skin Permeation log K_p ($cm \cdot s^{-1}$)	CYP1A2	CYP2C19	CYP2C9	CYP2D6	CYP3A4
8	High	No	Yes	-7.13	No	Yes	Yes	Yes	Yes
8A	High	No	No	-6.61	No	Yes	Yes	No	Yes
8B	High	No	Yes	-7.17	No	Yes	Yes	Yes	Yes
8C	Low	No	Yes	-7.46	No	Yes	Yes	No	Yes
8D	High	No	Yes	-6.93	No	Yes	Yes	Yes	Yes
8E	Low	No	Yes	-7.24	No	Yes	Yes	No	Yes
8F	High	No	No	-6.66	No	Yes	Yes	Yes	Yes
8G	High	No	Yes	-7.08	No	Yes	Yes	No	Yes
8H	High	No	Yes	-7.17	No	Yes	Yes	Yes	Yes
8I	Low	No	Yes	-7.70	Yes	Yes	Yes	Yes	Yes
8J	High	No	Yes	-6.93	No	Yes	Yes	No	Yes
8K	High	No	Yes	-6.70	No	Yes	Yes	Yes	Yes
8L	High	No	Yes	-7.42	No	Yes	Yes	No	Yes
8M	High	No	Yes	-6.88	No	Yes	Yes	No	Yes
VRV	High	No	No	-6.21	Yes	No	Yes	No	Yes
Doxorubicin	Low	No	Yes	-8.37	No	No	No	No	No
Tamoxifen	Low	No	Yes	-3.50	No	Yes	No	Yes	No

Table 9. Toxicity report and oral toxicity of cyanopyridine derivatives analyzed by the Protox III web server

Drug candidate	Toxicity End Points				Organ Toxicity				Predicted LD_{50} (mg/kg)	Predicted Toxicity class
	Cytotoxicity (P)	Carcinogenicity (P)	Immunotoxicity (P)	Cardiotoxicity (P)	Nephrotoxicity (P)	Hepatotoxicity (P)	Neurotoxicity (P)	Respiratory toxicity (P)		
8	Inactive (0.65)	Inactive (0.57)	Inactive (0.81)	Inactive (0.69)	Active (0.58)	Active (0.55)	Active (0.65)	Active (0.60)	400	4
8A	Inactive (0.66)	Inactive (0.68)	Inactive (0.95)	Inactive (0.79)	Active (0.53)	Inactive (0.51)	Active (0.85)	Active (0.69)	5000	5
8B	Inactive (0.65)	Inactive (0.58)	Inactive (0.97)	Inactive (0.69)	Active (0.51)	Active (0.55)	Active (0.74)	Active (0.65)	400	4
8C	Inactive (0.69)	Inactive (0.57)	Inactive (0.85)	Inactive (0.72)	Active (0.50)	Inactive (0.51)	Active (0.65)	Active (0.66)	400	4
8D	Inactive (0.66)	Inactive (0.58)	Inactive (0.56)	Inactive (0.69)	Active (0.51)	Active (0.55)	Active (0.74)	Active (0.65)	400	4
8E	Inactive (0.66)	Inactive (0.62)	Inactive (0.86)	Inactive (0.69)	Active (0.64)	Active (0.51)	Active (0.63)	Active (0.62)	400	4
8F	Inactive (0.67)	Inactive (0.59)	Inactive (0.84)	Inactive (0.71)	Active (0.54)	Active (0.52)	Active (0.72)	Active (0.65)	5000	5
8G	Inactive (0.54)	Inactive (0.64)	Inactive (0.94)	Inactive (0.77)	Active (0.53)	Inactive (0.54)	Active (0.81)	Active (0.69)	375	4
8H	Inactive (0.66)	Inactive (0.58)	Inactive (0.95)	Inactive (0.69)	Active (0.51)	Active (0.55)	Active (0.74)	Active (0.65)	375	4
8I	Inactive (0.66)	Inactive (0.59)	Inactive (0.99)	Inactive (0.68)	Active (0.55)	Inactive (0.51)	Active (0.67)	Active (0.61)	400	4
8J	Inactive (0.64)	Inactive (0.58)	Inactive (0.88)	Inactive (0.70)	Active (0.56)	Inactive (0.50)	Active (0.65)	Active (0.60)	1500	4
8K	Inactive (0.65)	Inactive (0.57)	Inactive (0.94)	Inactive (0.70)	Active (0.60)	Inactive (0.51)	Active (0.63)	Active (0.59)	5000	5
8L	Inactive (0.65	Inactive (0.62)	Inactive (0.96)	Inactive (0.80)	Active (0.50)	Inactive (0.54)	Active (0.79)	Active (0.78)	375	4
8M	Inactive (0.64)	Inactive (0.666)	Inactive (0.88)	Inactive (0.78)	Active (0.51)	Active (0.51)	Active (0.86)	Active (0.69)	1500	4
VRV	Inactive (0.85)	Active (0.52)	Inactive (0.98)	Inactive (0.84)	Active (0.57)	Active (0.57)	Active (0.67)	Active (0.64)	300	3
Doxorubicin	Active (0.94)	Inactive (0.90)	Active (0.99)	Active (0.64)	Active (0.80)	Inactive (0.86)	Active (0.74)	Active (0.91)	205	3
Tamoxifen	Inactive (0.93)	Inactive (0.62)	Active (0.96)	Inactive (0.77)	Inactive (0.90)	Inactive (0.51)	Active (0.87)	Active (0.98)	1190	4

P: Probability

The localization of compounds within the white region of the Boiled-Egg plot indicates high potential gastrointestinal absorption. This characteristic is observed in multiple cyanopyridine derivatives (8, 8A-B, 8D, 8F-H, 8J-N) as well as the native ligand and reference drug tamoxifen. On the other hand, the orange region in the Boiled-Egg plot represents compounds capable of passive BBB penetration [57]. In contrast, derivatives positioned outside both orange and white zones (8C, 8E, 8I) exhibit pronounced hydrophilicity, attributable to their amine (-NH_2) and hydroxyl (-OH) substituents. This high polarity significantly reduces their membrane diffusion potential, limiting bioavailability.

3.3. Toxicity Prediction

Toxicity predictions for cyanopyridine derivatives were performed using the Protox 3.0 web server. This stage is required in a series of drug design and development processes. The toxicity parameters in this study include endpoints such as cytotoxicity, carcinogenicity, and immunotoxicity. Then, organ toxicity, for instance, cardiotoxicity, hepatotoxicity, neurotoxicity, nephrotoxicity, and respiratory toxicity. Additionally, there are outputs for LD_{50} and toxicity classes. Table 9 presents the toxicity parameters of cyanopyridine derivatives, including the designed molecules, alongside native ligand and conventional breast cancer drugs such as Doxorubicin and Tamoxifen.

The analysis of potential human organ toxicity indicates that all cyanopyridine derivatives pose no risk to heart health (probability: 0.68-0.79). These derivatives are non-carcinogenic and demonstrate relative safety for cells (probability: 0.54 - 0.69) and the immune system (probability: 0.84 - 0.99). However, they exhibit potential hepatotoxicity, nephrotoxicity, and adverse effects on the nervous and respiratory systems. Similar conditions occur on Doxorubicin and Tamoxifen, with a high probability of 56–80%, as well as native ligand with a low probability of 57–67%.

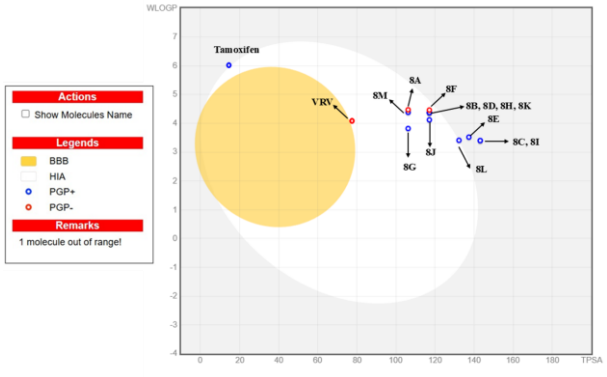

Figure 2. Boiled-Egg appearance of designed cyanopyridine derivatives, native ligand, and Tamoxifen

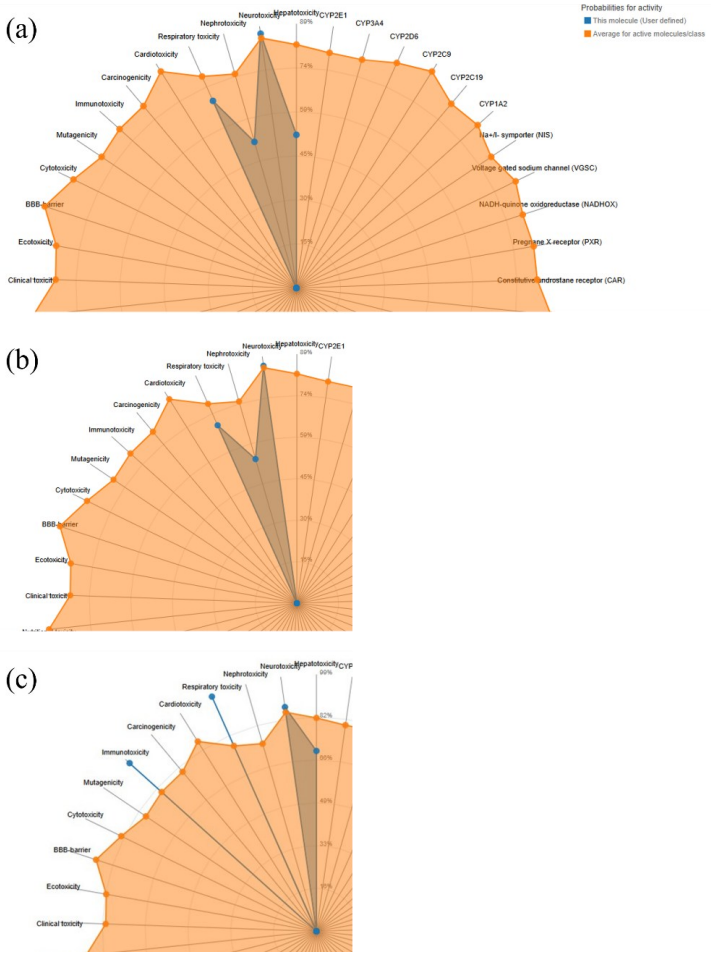

Figure 3. Toxicity radar of the comp. 8M (a; class 4), 8A (b; class 5), and Tamoxifen (c; class 4)

The toxicity classification of cyanopyridine derivatives is divided into two categories: class 4 and class 5. Compounds 8A, 8F, and 8K are classified in class 5, indicating lower toxicity than other derivatives, with the highest LD_{50} of 5000 mg/kg. Drug compounds in class 5 ($2000 < LD_{50} \leq 5000$ mg/kg) reveal minimal toxicity in mice and are considered relatively safe for humans. The remaining derivatives, including Tamoxifen, are categorized under class 4, which has a lower LD_{50} range ($300 < LD_{50} \leq 2000$) and thus presents a higher toxicity risk. The toxicity profiles of selected cyanopyridine derivatives, representing each class, are illustrated in Figure 4. Meanwhile, VRV and another conventional drug, doxorubicin, fall under class 3 ($50 < LD_{50} \leq 300$ mg/kg), indicating their harmful nature in humans.

3.4. Docking Molecular and Molecular Dynamics Simulation Studies

The docking protocol was validated by redocking the native ligand (6-(5-bromo-2-hydroxy-phenyl)-2-oxo-4-phenyl-1H-pyridine-3-carbonitrile, or VRV) into the PIM-1 kinase receptor to verify methodological accuracy. Nine distinct VRV conformations were obtained, each conformation exhibiting RMSD values below 2 Å and binding affinities ranging from -9.0 to -9.2 kcal·mol^{-1}. These RMSD values confirm minimal positional deviation from the crystallographic reference structure, indicating satisfactory reproduction of the native binding pose. The calculated binding energies of these reference conformations subsequently served as benchmarks for evaluating the designed cyanopyridine derivatives. Figure 4 displays the orientation of the native ligand before and after redocking procedures.

Furthermore, the designed molecules, serving as test ligands, were docked to the PIM-1 kinase receptor to investigate their interactions. Docking results show strong binding to the receptor. Compound 8E forms one conventional hydrogen bond with an amino acid residue. Other compounds showing conventional hydrogen bonds in the 2D interaction analysis (Figure 5) are VRV, doxorubicin, and compound 8. These interactions are further stabilized by ionic interactions, particularly π–anion and π–cation interactions, enhancing binding specificity and stability. Conversely, tamoxifen and designed derivatives (8A, 8L, and 8M) do not form conventional hydrogen bonds with the receptor, indicating weaker interactions. However, 8M exhibits a strong halogen interaction with glutamic acid. These results agree with the binding affinity data in Table 10, where more negative ΔG values (-9.4 to -9.7 kcal·mol^{-1}) indicate stronger ligand–receptor binding [58]. This enhanced binding directly correlates with improved antiproliferative efficacy.

Additional stabilizing interactions, including π-π stacking, π-alkyl, and C-H bonds, further contribute to PIM-1 kinase inhibition [35], consistent with the computationally predicted IC_{50} values. The binding affinities have negative values, representing the spontaneity of the interaction between designed ligands and the receptor. Notably, all designed compounds exhibit significantly more negative binding energies than both VRV and tamoxifen and are close to doxorubicin. This reflects their enhanced inhibitory potential against breast cancer targets. Based on these robust computational results, derivative 8M emerges as a prime candidate for experimental validation through chemical synthesis and biological evaluation. While demonstrating promising binding characteristics, the current results have not yet surpassed the reported affinities of established FDA-approved compounds (rifaximin, stanozolol, telmisartan, alfaxalone) for PIM-1 kinase. Those reference compounds exhibit superior binding energies reaching -13 kcal·mol^{-1} [59], suggesting our derivatives require further optimization to achieve comparable potency.

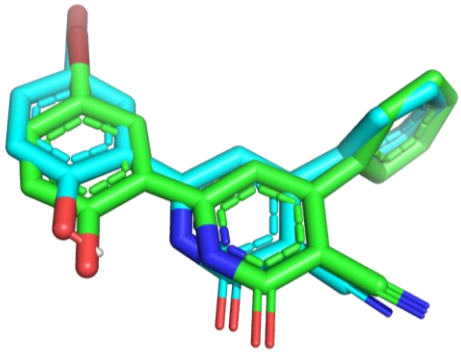

Figure 4. The overlap between the native ligands before (cyan blue) and after redocking (green)

Table 10. Docking molecular results of PIM-1 kinase receptor with native ligand, positive control, and designed molecules

Ligand	Binding Affinity (kcal·mol^{-1})	RMSD (Å)	Hydrogen bond interactions
VRV (Native)	-9.2	1.365	LYS A67
Tamoxifen (Positive control)	-8.0	0.0	-
Doxorubicin (Positive control)	-10.0	0.0	ASP A128, SER A46
8	-9.2	0.0	ASP A128, LYS A67, GLU A121
8A	-9.5	0.0	-
8E	-9.6	0.0	LYS A67
8L	-9.4	0.0	-
8M	-9.7	0.0	-

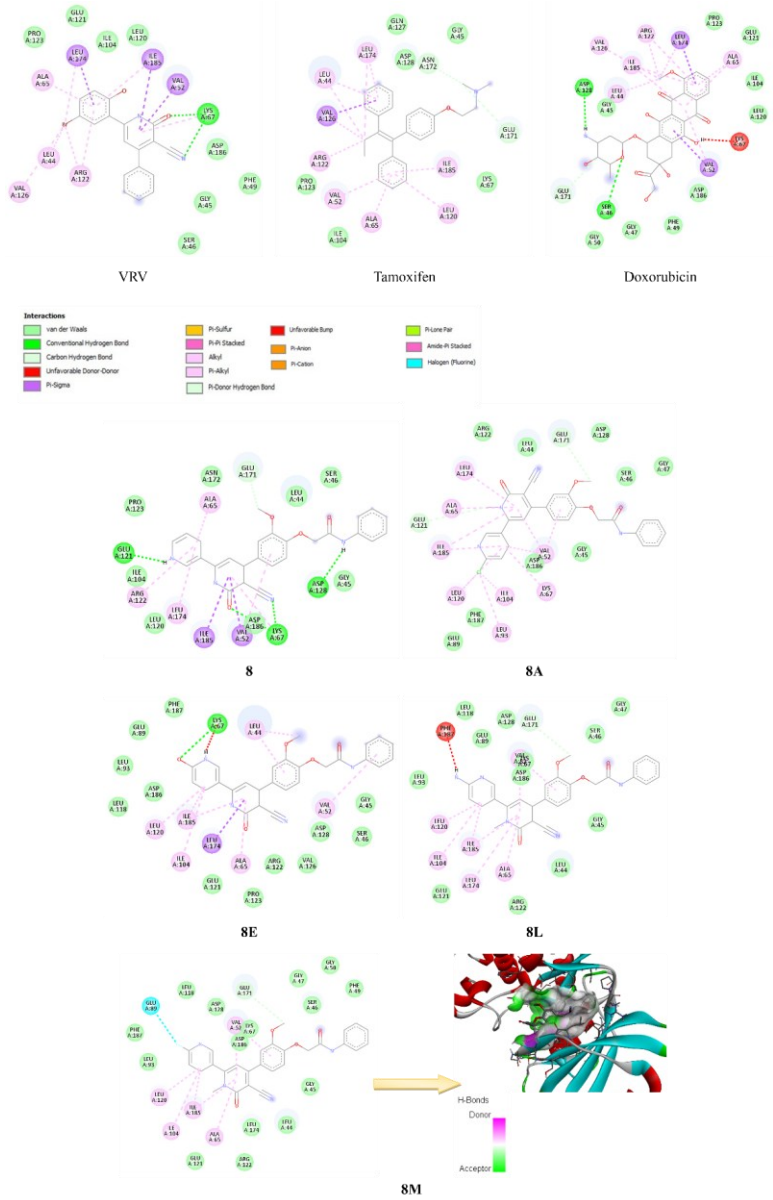

Figure 5. 2D visualization on the interaction of VRV (natural ligand), Tamoxifen (positive controls), Doxorubicin (positive controls), compound 8, and designed molecules (8A, 8E, 8L, and 8M) with PIM-1 kinase receptor (PDB ID: 2OBJ)

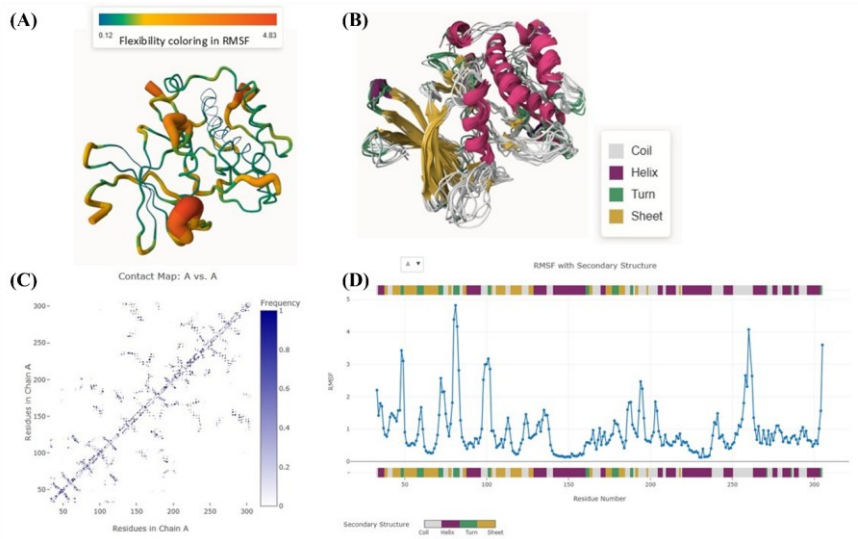

Figure 6. (A) Flexibility coloring in RMSF, (B) all models of PIM-1 kinase receptor, (C) contact map, and (D) RMSF profiles of all residues from CABS-flex III simulation

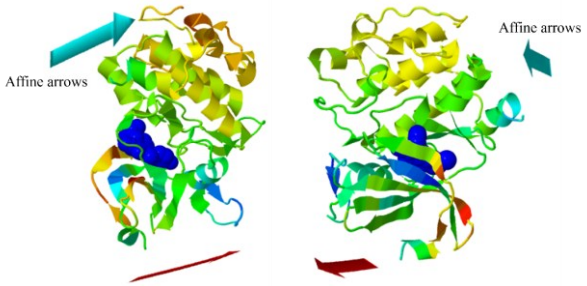

Figure 7. Molecular mobility of the PIM-1 kinase-8M (left) and PIM-1 kinase-VRV (right) evaluated by iMODS

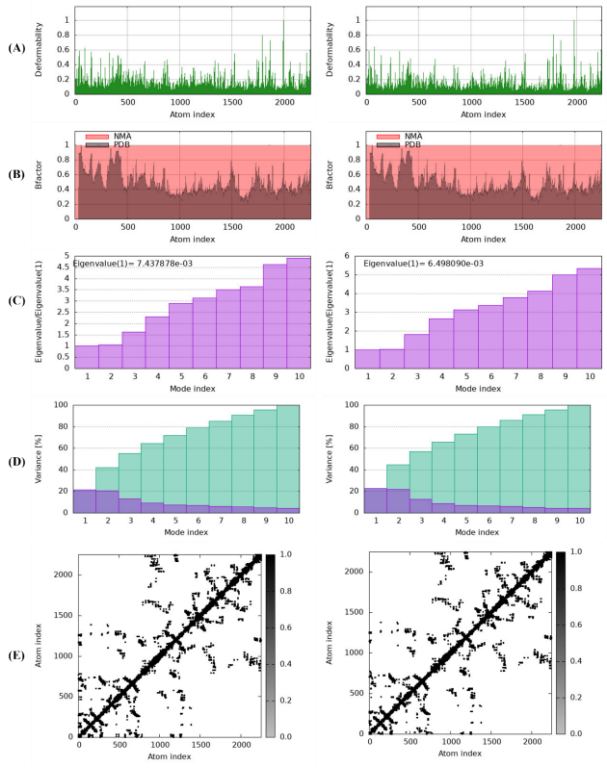

Figure 8. Outputs of molecular dynamics simulation using iMODS for PIM-1 kinase–8M (left) and PIM-kinase-VRV (right): (A) Deformability graphs, (B) B- factor plots, (C) Eigenvalue plots, (D) variance map plots, and (E) elastic network plots

The molecular dynamics simulation of PIM-1 kinase receptor was performed using the CABS-flex III web server, generating ten overlapping structural models (Figure 6B). The root mean square fluctuation (RMSF) profile (Figure 6D) showed residue flexibility, where higher values indicate greater mobility and lower values indicate rigidity [60]. Protein conformational flexibility, a key determinant of biological function, influences ligand binding [61]. Quantitative evaluation of RMSF profiles revealed differential residue flexibility, with residue 231 exhibiting minimal structural displacement (0.127 Å) compared to the pronounced conformational mobility of residue 81 (4.821 Å). The average RMSF of 0.9382 Å suggests overall structural stability, with most residues demonstrating fluctuations within the 3 Å threshold for stable folded proteins [62]. The contact map derived from CABS-flex simulations (Figure 6C) illustrates inter-residue spatial relationships [32], where increasing colorimetric intensity (blue gradient) correlates with interaction persistence and structural stabilization throughout the 1 µs simulation trajectory.

The physical dynamics and stability of the docked complexes were assessed using iMODS through NMA, which characterizes low-frequency motions and reveals significant conformational flexibility. Figure 7 illustrates the molecular mobility of the PIM-1 kinase receptor when bound to compounds 8M and VRV, where affine arrows (color-coded by magnitude) indicate directional movement, and longer arrows denote higher mobility. The receptor's structural flexibility is further represented by a color gradient: blue (stiff, low flexibility), green (intermediate flexibility), and yellow (highly dynamic regions).

Additional analyses (Figure 8) include deformability graphs and B-factor plots, which reflect residue-specific deformability and mobility, respectively. Peaks in the deformability graph correspond to regions of heightened structural plasticity [63]. Eigenvalue analysis revealed the energy required for complex deformation, with higher values (PIM-1 kinase – 8M: 7.438×10^{-3}; PIM-1 kinase – VRV: 6.498×10^{-3}). This indicates that the complex of PIM-1 kinase – 8M possesses greater stiffness and requires higher deformation energy. Consequently, the complex can be interpreted as more stable through reinforced PIM-1 kinase–8M interactions. The atom index map further resolved motion correlations between residues, with black regions signifying correlated movements and white indicating anticorrelated motions. Compound 8M exhibited stiffer and stronger correlations (more intense black) than VRV, suggesting more synchronized residue dynamics. Collectively, these results position compound 8M as a promising antiproliferative candidate due to its enhanced stability, flexibility, and interaction profile.

3.5. Limitations

The semi-empirical PM3 method was implemented in this study. Although PM3 was suitable for this comparative QSAR study, higher-level DFT methods are more recommended for determining absolute properties in future work using advanced software like Orca or Gaussian. The obtained QSAR equations exhibit broad applicability for various cyanopyridine derivatives. Nevertheless, the optimal QSAR model (Model 1) relies solely on net atomic charges as descriptors, as other evaluated parameters, including electronic, steric, and hydrophobic properties, demonstrated no statistically significant correlation with antiproliferative activity. The results of external validation indicate that two parameters, the R^2 and R^2_{ext}, did not approach 1. This indicates that the correlation of calculated

antiproliferative and structural parameters is not highly significant. In terms of the toxicity of designed compounds utilizing protox III, several toxicity endpoints, such as cytotoxicity and carcinogenicity, have a moderate probability, which is similar to nephrotoxicity, hepatotoxicity, and respiratory toxicity in organ toxicity. Thus, these analyses should be investigated further. Due to the application of an *in silico* approach, these results should be supported by *in vitro* and *in vivo* studies to reveal the efficacy, toxicity, and bioavailability of the designed cyanopyridine derivatives.

4. Conclusion

The quantitative structure-activity relationship (QSAR) of cyanopyridine derivatives was analyzed using the PM3 semi-empirical method, yielding Model 1 as the best QSAR equation ($\log(1/IC_{50}) = 151.273 + 1884.726qC_1 - 4663.478qC_4 + 5431.564qC_5 + 1501.074qN_7 + 592.015qO_{10}$). Based on this model, new derivatives were designed, exhibiting enhanced antiproliferative activity compared to previously synthesized analogs. Among them, compound 8M demonstrated superior predicted bioactivity (lower IC_{50}) and binding affinity, relative to other cyanopyridine derivatives. *In silico* pharmacokinetics and toxicity assessments revealed that 8M possesses a relatively good pharmacokinetics profile and toxicity. Drug-likeness and pharmacokinetic evaluations of these molecules confirmed compliance with Lipinski's, Egan's, Muegge's, and Veber's rules. Molecular docking analysis indicated binding affinities of the modified derivatives comparable to the native ligand. This is supported by the results obtained from molecular dynamics simulations. Therefore, designed molecules from cyanopyridine derivatives represent promising candidates for future utilization and development as anti-breast cancer agents. These findings provide a rational basis for other designs, synthesizing, and experimentally validating these compounds through *in vitro* and *in vivo* studies to assess their antiproliferative potential.

Acknowledgement

This research was fully supported by the Directorate of Research and Community Service, Kementerian Pendidikan Tinggi, Sains, dan Teknologi, through the Basic Research Scheme (Penelitian Dosen Pemula) in 2025 with the grant number: 106/C3/DT.05.00.PL/2025 and Universitas Sembilanbelas November Kolaka with contract number: 87/UN56.D.01/PN.03.00/2025.

References

[1] Nadia Harbeck, Frédérique Penault-Llorca, Javier Cortes, Michael Gnant, Nehmat Houssami, Philip Poortmans, Kathryn Ruddy, Janice Tsang, Fatima Cardoso, Breast cancer, *Nature Reviews Disease Primers*, 5, 1, (2019), 66 https://doi.org/10.1038/s41572-019-0111-2

[2] Angela N. Giaquinto, Hyuna Sung, Kimberly D. Miller, Joan L. Kramer, Lisa A. Newman, Adair Minihan, Ahmedin Jemal, Rebecca L. Siegel, Breast Cancer Statistics, 2022, *CA: A Cancer Journal for Clinicians*, 72, 6, (2022), 524-541 https://doi.org/10.3322/caac.21754

[3] Kimberly D. Miller, Leticia Nogueira, Theresa Devasia, Angela B. Mariotto, K. Robin Yabroff, Ahmedin Jemal, Joan Kramer, Rebecca L. Siegel, Cancer treatment and survivorship statistics, 2022, *CA: A Cancer Journal for Clinicians*, 72, 5, (2022), 409-436 https://doi.org/10.3322/caac.21731

[4] Natascia Marino, Stephan Woditschka, L. Tiffany Reed, Joji Nakayama, Musa Mayer, Maria Wetzel, Patricia S. Steeg, Breast Cancer Metastasis: Issues for the Personalization of Its Prevention and Treatment, *The American Journal of Pathology*, 183, 4, (2013), 1084-1095 https://doi.org/10.1016/j.ajpath.2013.06.012

[5] Jesse Yu, Qingxin Mu, Millie Fung, Xiaolin Xu, Linxi Zhu, Rodney J. Y. Ho, Challenges and opportunities in metastatic breast cancer treatments: Nano-drug combinations delivered preferentially to metastatic cells may enhance therapeutic response, *Pharmacology & Therapeutics*, 236, (2022), 108108 https://doi.org/10.1016/j.pharmthera.2022.108108

[6] Yuening Xiang, Zimu Guo, Pengfei Zhu, Jia Chen, Yongye Huang, Traditional Chinese medicine as a cancer treatment: Modern perspectives of ancient but advanced science, *Cancer Medicine*, 8, 5, (2019), 1958-1975 https://doi.org/10.1002/cam4.2108

[7] Nagesh Kishan Panchal, E. P. Sabina, A serine/threonine protein PIM kinase as a biomarker of cancer and a target for anti-tumor therapy, *Life Sciences*, 255, (2020), 117866 https://doi.org/10.1016/j.lfs.2020.117866

[8] Cristina Ferreira Almeida, Ana Oliveira, Maria João Ramos, Pedro A. Fernandes, Natércia Teixeira, Cristina Amaral, Estrogen receptor-positive (ER^+) breast cancer treatment: Are multi-target compounds the next promising approach?, *Biochemical Pharmacology*, 177, (2020), 113989 https://doi.org/10.1016/j.bcp.2020.113989

[9] Hadiza Lawal Abdulrahman, Adamu Uzairu, Sani Uba, Computer modeling of some anti-breast cancer compounds, *Structural Chemistry*, 32, 2, (2021), 679-687 https://doi.org/10.1007/s11224-020-01608-7

[10] Hadiza Lawal Abdulrahman, Adamu Uzairu, Sani Uba, QSAR, Ligand Based Design and Pharmacokinetic Studies of Parviflorons Derivatives as Anti-Breast Cancer Drug Compounds Against MCF-7 Cell Line, *Chemistry Africa*, 4, 1, (2021), 175-187 https://doi.org/10.1007/s42250-020-00207-7

[11] Mohammed Albratty, Hassan Ahmad Alhazmi, Novel pyridine and pyrimidine derivatives as promising anticancer agents: A review, *Arabian Journal of Chemistry*, 15, (2022), 103846 https://doi.org/10.1016/j.arabjc.2022.103846

[12] Muhammad Akbar S. Kurniawan, Muhamad Jalil Baari, Sariyanti Sariyanti, Finarisnawati Finarisnawati, QSAR Analysis Using Semi-Empirical AM1 Method, Molecular Docking, and ADMET Studies of Chalcone Derivatives as Antimalarial Compounds, *Jurnal Kimia Riset*, 8, 2, (2023), 186-199 https://doi.org/10.20473/jkr.v8i2.51798

[13] Abdulrahman Ibrahim Kubo, Adamu Uzairu, Ibrahim Tijjani Babalola, Muhammad Tukur Ibrahim, Abdullahi Bello Umar, QSAR, molecular docking, and pharmacokinetic analysis of thiosemicarbazone-indole compounds targeting prostate cancer cells, *Journal of Taibah University*

Medical Sciences, 19, 4, (2024), 823-834 https://doi.org/10.1016/j.jtumed.2024.07.004

[14] Adinda Adelia Wulandari, Achmad Aziz Choiri, Fitria, Tri Widiandani, Thymoquinone and its derivatives against breast cancer with HER2 positive: *in silico* studies of ADMET, docking and QSPR, *Journal of Basic and Clinical Physiology and Pharmacology*, 32, 4, (2021), 393-401 https://doi.org/10.1515/jbcpp-2020-0431

[15] Mona H. Ibrahim, Marwa F. Harras, Shaimaa K. Mostafa, Salma M. Mohyeldin, Omkulthom Al kamaly, Najla Altwaijry, Rehab Sabour, Development of novel cyanopyridines as PIM-1 kinase inhibitors with potent anti-prostate cancer activity: Synthesis, biological evaluation, nanoparticles formulation and molecular dynamics simulation, *Bioorganic Chemistry*, 129, (2022), 106122 https://doi.org/10.1016/j.bioorg.2022.106122

[16] Patrycja Wińska, Monika Wielechowska, Mirosława Koronkiewicz, Paweł Borowiecki, Synthesis and Anticancer Activity of Novel Dual Inhibitors of Human Protein Kinases CK2 and PIM-1, *Pharmaceutics*, 15, 7, (2023), 1991 https://doi.org/10.3390/pharmaceutics15071991

[17] Bahgat R. M. Hussein, Hayam H. Mohammed, Eman A. Ahmed, Omar Alshazly, Mamdouh F. A. Mohamed, Omran A. Omran, Design, synthesis, and anti-breast cancer activity evaluation of novel 3-cyanopyridine derivatives as PIM-1 inhibitors, *Molecular Diversity*, 29, 3, (2025), 2565-2584 https://doi.org/10.1007/s11030-024-11010-8

[18] Brian J. Bennion, Nicholas A. Be, M. Windy McNerney, Victoria Lao, Emma M. Carlson, Carlos A. Valdez, Michael A. Malfatti, Heather A. Enright, Tuan H. Nguyen, Felice C. Lightstone, Timothy S. Carpenter, Predicting a Drug's Membrane Permeability: A Computational Model Validated With *in Vitro* Permeability Assay Data, *The Journal of Physical Chemistry B*, 121, 20, (2017), 5228-5237 https://doi.org/10.1021/acs.jpcb.7b02914

[19] Mark Froimowitz, HyperChem: a software package for computational chemistry and molecular modeling, *BioTechniques*, 14, 6, (1993), 1010-1013

[20] Agus Dwi Ananto, Handa Muliasari, Saprizal Hadisaputra, Design New Compound of Meisoindigo Derivative as Anti Breast Cancer Based on QSAR Approach, *Jurnal Kimia Sains dan Aplikasi*, 23, 9, (2020), 305-311 https://doi.org/10.14710/jksa.23.9.305-311

[21] Khusna Arif Rakhman, Nur Asbirayani Limatahu, Hasbul Budiman Karim, Muhammad Ikhlas Abdjan, Kajian Senyawa Turunan Benzopirazin sebagai Antimalaria Menggunakan Metode HKSA dan MLR, *EduChemia: Jurnal Kimia dan Pendidikan*, 4, 2, (2019), 112-126 https://dx.doi.org/10.30870/educhemia.v4i2.4989

[22] Jufrizal Syahri, Bambang Purwono, Ria Armunanto, Design of new potential antimalaria compound based on QSAR analysis of chalcone derivatives, *International Journal of Pharmaceutical Sciences Review and Research*, 36, 2, (2016), 71-76

[23] Antoine Daina, Olivier Michielin, Vincent Zoete, SwissADME: a free web tool to evaluate pharmacokinetics, drug-likeness and medicinal chemistry friendliness of small molecules, *Scientific Reports*, 7, 1, (2017), 42717 https://doi.org/10.1038/srep42717

[24] Antoine Daina, Vincent Zoete, A BOILED-Egg To Predict Gastrointestinal Absorption and Brain Penetration of Small Molecules, *ChemMedChem*, 11, 11, (2016), 1117-1121 https://doi.org/10.1002/cmdc.201600182

[25] Priyanka Banerjee, Emanuel Kemmler, Mathias Dunkel, Robert Preissner, ProTox 3.0: a webserver for the prediction of toxicity of chemicals, *Nucleic Acids Research*, 52, W1, (2024), W513-W520 https://doi.org/10.1093/nar/gkae303

[26] Dassault Systèmes, *BIOVIA, Discovery Studio Modeling Environment*, Dassault Systèmes Biovia, San Diego, CA, USA, 2016,

[27] Shakeel Ahmad Khan, Ying Wu, Amy Sze-Man Li, Xiu-Qiong Fu, Zhi-Ling Yu, Network pharmacology and molecular docking-based prediction of active compounds and mechanisms of action of Cnidii Fructus in treating atopic dermatitis, *BMC Complementary Medicine and Therapies*, 22, 1, (2022), 275 https://doi.org/10.1186/s12906-022-03734-7

[28] Sargis Dallakyan, Arthur J. Olson, Small-Molecule Library Screening by Docking with PyRx, in: *Chemical biology: methods and protocols*, Springer, 2014, https://doi.org/10.1007/978-1-4939-2269-7_19

[29] Sree Karani Kondapuram, Sailu Sarvagalla, Mohane Selvaraj Coumar, Chapter 22 - Docking-Based Virtual Screening Using PyRx Tool: Autophagy Target Vps34 as a Case Study, in: M.S. Coumar (Ed.) *Molecular Docking for Computer-Aided Drug Design*, Academic Press, 2021, https://doi.org/10.1016/B978-0-12-822312-3.00019-9

[30] Bakary N'tji Diallo, Tarryn Swart, Heinrich C. Hoppe, Özlem Tastan Bishop, Kevin Lobb, Potential repurposing of four FDA approved compounds with antiplasmodial activity identified through proteome scale computational drug discovery and in vitro assay, *Scientific Reports*, 11, 1, (2021), 1413 https://doi.org/10.1038/s41598-020-80722-2

[31] Wei P. Feinstein, Michal Brylinski, Calculating an optimal box size for ligand docking and virtual screening against experimental and predicted binding pockets, *Journal of Cheminformatics*, 7, 1, (2015), 18 https://doi.org/10.1186/s13321-015-0067-5

[32] Karol Wróblewski, Mateusz Zalewski, Aleksander Kuriata, Sebastian Kmiecik, CABS-flex 3.0: an online tool for simulating protein structural flexibility and peptide modeling, *Nucleic Acids Research*, 53, W1, (2025), W95-W101 https://doi.org/10.1093/nar/gkaf412

[33] José Ramón López-Blanco, José I. Aliaga, Enrique S. Quintana-Ortí, Pablo Chacón, iMODS: internal coordinates normal mode analysis server, *Nucleic Acids Research*, 42, W1, (2014), W271-W276 https://doi.org/10.1093/nar/gku339

[34] Harno Dwi Pranowo, *Pengantar Kimia Komputasi*, Austrian-Indonesian Centre for Computational Chemistry (AIC), Yogyakarta, 2022,

[35] S. S. W. Waskitha, F. E. Mulyana, N. F. Riza, Y. M. Stansyah, I. Tahir, T. D. Wahyuningsih, QSAR

approach and synthesis of chalcone derivatives as antimalarial compound against *Plasmodium falciparum* 3D7 Strain, *Rasayan Journal of Chemistry*, 14, 4, (2021), p2363 https://doi.org/10.31788/RJC.2021.1445867

[36] Nabil Bouarra, Soumaya Kherouf, Nawel Nadji, Loubna Nouri, Amel Boudjemaa, Souad Djerad, Khaldoun Bachari, Quantitative structure-electrochemistry relationship modeling of a series of anticancer agents using MLR and ANN approaches, *Chemical Product and Process Modeling*, 19, 2, (2024), 251-262 https://doi.org/10.1515/cppm-2023-0024

[37] Alexander Tropsha, Chapter 2 - Development of QSAR models as reliable computational tools for regulatory assessment of chemicals for acute toxicity, in: H. Hong (Ed.) *QSAR in Safety Evaluation and Risk Assessment*, Academic Press, 2024, https://doi.org/10.1016/B978-0-443-15339-6.00003-5

[38] Saudatu Chinade Ja'afaru, Adamu Uzairu, Renato Araújo da Costa, Muhammed Sani Sallau, Muhammad Tukur Ibrahim, Ligand-based virtual screening and QSAR modelling for the discovery of potent SmHDAC8 inhibitors, *In Silico Research in Biomedicine*, 1, (2025), 100044 https://doi.org/10.1016/j.insi.2025.100044

[39] Saudatu C. Ja'afaru, Adamu Uzairu, Anshuman Chandra, Muhammed S. Sallau, George I. Ndukwe, Muhammad T. Ibrahim, Imteyaz Qamar, Ligand based-design of potential schistosomiasis inhibitors through QSAR, homology modeling, molecular dynamics, pharmacokinetics, and DFT studies, *Journal of Taibah University Medical Sciences*, 19, 2, (2024), 429-446 https://doi.org/10.1016/j.jtumed.2024.02.003

[40] T. Brintha, J. Jeni James, M. Amalanathan, P. J. Jegan Babu, M. Sony Michael Mary, Experimental and theoretical investigation of structure activity relationship on L-Lysine Monohydrate for antioxidant efficacy, *Chemical Physics Impact*, 7, (2023), 100311 https://doi.org/10.1016/j.chphi.2023.100311

[41] David Dahlgren, Biopharmaceutical aspects of intestinal drug absorption: Regional permeability and absorption-modifying excipients, *Doctoral thesis, comprehensive summary*, Digital Comprehensive Summaries of Uppsala Dissertations from the Faculty of Pharmacy, Acta Universitatis Upsaliensis, Uppsala, 2018

[42] Christopher A. Lipinski, Franco Lombardo, Beryl W. Dominy, Paul J. Feeney, Experimental and computational approaches to estimate solubility and permeability in drug discovery and development settings 1PII of original article: S0169-409X(96)00423-1. The article was originally published in Advanced Drug Delivery Reviews 23 (1997) 3–25.1, *Advanced Drug Delivery Reviews*, 46, 1, (2001), 3-26 https://doi.org/10.1016/S0169-409X(00)00129-0

[43] Shuzhe Wang, Gerhard König, Hans-Jörg Roth, Marianne Fouché, Stephane Rodde, Sereina Riniker, Effect of Flexibility, Lipophilicity, and the Location of Polar Residues on the Passive Membrane Permeability of a Series of Cyclic Decapeptides, *Journal of Medicinal Chemistry*, 64, 17, (2021), 12761-12773 https://doi.org/10.1021/acs.jmedchem.1c00775

[44] Daniel H. O' Donovan, Claudia De Fusco, Lara Kuhnke, Andreas Reichel, Trends in Molecular Properties, Bioavailability, and Permeability across the Bayer Compound Collection, *Journal of Medicinal Chemistry*, 66, 4, (2023), 2347-2360 https://doi.org/10.1021/acs.jmedchem.2c01577

[45] Elara Voss, Drug Absorption: A Critical Aspect of Biopharmaceutics, *Journal of Basic and Clinical Pharmacy*, 15, 4, (2024), 365-366

[46] Longfei Guan, Hongbin Yang, Yingchun Cai, Lixia Sun, Peiwen Di, Weihua Li, Guixia Liu, Yun Tang, ADMET-score – a comprehensive scoring function for evaluation of chemical drug-likeness, *MedChemComm*, 10, 1, (2019), 148-157 https://doi.org/10.1039/c8md00472b

[47] M. T. Mahanthesh, D. Ranjith, R. Yaligar, R. Jyothi, G. Narappa, M. Ravi, Swiss ADME prediction of phytochemicals present in *Butea monosperma* (Lam.) Taub, *Journal of Pharmacognosy and Phytochemistry*, 9, 3, (2020), 1799-1809

[48] Arup K. Ghose, Vellarkad N. Viswanadhan, John J. Wendoloski, A Knowledge-Based Approach in Designing Combinatorial or Medicinal Chemistry Libraries for Drug Discovery. 1. A Qualitative and Quantitative Characterization of Known Drug Databases, *Journal of Combinatorial Chemistry*, 1, 1, (1999), 55-68 https://doi.org/10.1021/cc9800071

[49] William J. Egan, Kenneth M. Merz, John J. Baldwin, Prediction of Drug Absorption Using Multivariate Statistics, *Journal of Medicinal Chemistry*, 43, 21, (2000), 3867-3877 https://doi.org/10.1021/jm000292e

[50] Divvela Hema Nagadurga, Bioavailability and Bioequivalence Studies, in: U. Ahmad, J. Akhtar (Eds.) *Pharmaceutical Formulation Design - Recent Practices*, IntechOpen, London, 2019, https://doi.org/10.5772/intechopen.85145

[51] Yvonne C. Martin, A Bioavailability Score, *Journal of Medicinal Chemistry*, 48, 9, (2005), 3164-3170 https://doi.org/10.1021/jm0492002

[52] Shuan Chen, Yousung Jung, Estimating the synthetic accessibility of molecules with building block and reaction-aware SAScore, *Journal of Cheminformatics*, 16, 1, (2024), 83 https://doi.org/10.1186/s13321-024-00879-0

[53] Yoshifumi Fukunishi, Takashi Kurosawa, Yoshiaki Mikami, Haruki Nakamura, Prediction of Synthetic Accessibility Based on Commercially Available Compound Databases, *Journal of Chemical Information and Modeling*, 54, 12, (2014), 3259-3267 https://doi.org/10.1021/ci500568d

[54] Peter Ertl, Ansgar Schuffenhauer, Estimation of synthetic accessibility score of drug-like molecules based on molecular complexity and fragment contributions, *Journal of Cheminformatics*, 1, 1, (2009), 8 https://doi.org/10.1186/1758-2946-1-8

[55] Ionut Mădălin Gridan, Alecu Aurel Ciorsac, Adriana Isvoran, Prediction of ADME-Tox properties and toxicological endpoints of triazole fungicides used for cereals protection, *ADMET and DMPK*, 7, 3, (2019), 161-173 https://doi.org/10.5599/admet.668

[56] Madhu S. Singh, Prudence A. Francis, Michael Michael, Tamoxifen, cytochrome P450 genes and breast cancer clinical outcomes, *The Breast*, 20, 2,

(2011), 111-118
https://doi.org/10.1016/j.breast.2010.11.003

[57] Werner J. Geldenhuys, Afroz S. Mohammad, Chris E. Adkins, Paul R. Lockman, Molecular Determinants of blood–brain Barrier Permeation, *Therapeutic Delivery*, 6, 8, (2015), 961-971
https://doi.org/10.4155/tde.15.32

[58] Anna Yuliana, Ira Rahmiyani, Cindi Kartika, Molecular Docking and Molecular Dynamics Simulation using *Monascus* sp. as a Candidate Cervical Cancer Drug, *Journal of Tropical Pharmacy and Chemistry*, 7, 1, (2025), 41-51

[59] Aanchal Rathi, Saba Noor, Md Nayab Sulaimani, Shahbaz Ahmed, Aaliya Taiyab, Mohamed F. AlAjmi, Faez Iqbal Khan, Md Imtaiyaz Hassan, Mohammad Mahfuzul Haque, FDA-approved drugs as PIM-1 kinase inhibitors: A drug repurposed approach for cancer therapy, *International Journal of Biological Macromolecules*, 292, (2025), 139107
https://doi.org/10.1016/j.ijbiomac.2024.139107

[60] Sumera, Farha Anwer, Maaz Waseem, Areeba Fatima, Nishat Malik, Amjad Ali, Saadia Zahid, Molecular Docking and Molecular Dynamics Studies Reveal Secretory Proteins as Novel Targets of Temozolomide in Glioblastoma Multiforme, *Molecules*, 27, 21, (2022), 7198
https://doi.org/10.3390/molecules27217198

[61] Outi M. H. Salo-Ahen, Ida Alanko, Rajendra Bhadane, Alexandre M. J. J. Bonvin, Rodrigo Vargas Honorato, Shakhawath Hossain, André H. Juffer, Aleksei Kabedev, Maija Lahtela-Kakkonen, Anders Støttrup Larsen, Eveline Lescrinier, Parthiban Marimuthu, Muhammad Usman Mirza, Ghulam Mustafa, Ariane Nunes-Alves, Tatu Pantsar, Atefeh Saadabadi, Kalaimathy Singaravelu, Michiel Vanmeert, Molecular Dynamics Simulations in Drug Discovery and Pharmaceutical Development, *Processes*, 9, 1, (2021), 71
https://doi.org/10.3390/pr9010071

[62] Azra Sakhawat, Muhammad Umer Khan, Raima Rehman, Samiullah Khan, Muhammad Adnan Shan, Alia Batool, Muhammad Arshad Javed, Qurban Ali, Natural compound targeting *BDNF* V66M variant: insights from in silico docking and molecular analysis, *AMB Express*, 13, 1, (2023), 134
https://doi.org/10.1186/s13568-023-01640-w

[63] M. Yasser Alsedfy, A. A. Ebnalwaled, Mona Moustafa, Alaa Hassan Said, Investigating the binding affinity, molecular dynamics, and ADMET properties of curcumin-IONPs as a mucoadhesive bioavailable oral treatment for iron deficiency anemia, *Scientific Reports*, 14, 1, (2024), 22027
https://doi.org/10.1038/s41598-024-72577-8